Wind Structure in an Intermediate Boundary Layer Model Based on Ekman Momentum Approximation[1]

Tan Zhemin (谈哲敏)[2] and Wang Yuan (王 元)

Key Laboratory of Meso-Scale Severe Weather/ MOE, Department of Atmospheric Sciences, Nanjing University, Nanjing 210093

(Received March 26, 2001; revised September 5, 2001)

ABSTRACT

A quasi three-dimensional, intermediate planetary boundary layer (PBL) model is developed by including inertial acceleration with the Ekman momentum approximation, but a nonlinear eddy viscosity based on Blackadar's scheme was included to improve the theoretical model proposed by Tan and Wu (1993). The model could keep the same complexity as the classical Ekman model in numerical, but extends the conventional Ekman model to include the horizontal accelerated flow with the Ekman momentum approximation.

A comparison between this modified Ekman model and other simplified accelerating PBL models is made. Results show that the Ekman model overestimates (underestimates) the wind speed and pumping velocity in the cyclonic (anticyclonic) shear flow due to the neglect of the acceleration flow, however, the semi-geostrophic Ekman model overestimates the acceleration effects resulting from the underestimating (overestimating) of the wind speed and pumping velocity in the cyclonic (anticyclonic) shear flow. The Ekman momentum approximation boundary layer model could be applied to the baroclinic atmosphere. The baroclinic Ekman momentum approximation boundary layer solution has both features of classical baroclinic Ekman layer and the Ekman momentum approximate boundary lager.

Key words: Wind structure, Ekman momentum approximation, Boundary layer model

1. Introduction

A major challenge in the atmospheric dynamics and numerical atmospheric modeling is to adequately represent the unresolved physics of the boundary layer. The simplest boundary-layer model was first developed by Ekman (1905), which is called Ekman layer model (hereafter EK). In the Ekman model there is a balance among the pressure gradient force, the Coriolis force and the turbulent friction (Holton 1992). Therefore, the Ekman model is linear. Nevertheless, the Ekman model could describe the main dynamic process in the PBL, and gives a hodograph that veers with height with a cross-isobaric flow toward lower pressure near the surface that approaches to a geostrophic flow aloft.

In general the conventional PBL model often neglect the nonlinear advection or effect of background wind and pressure fields that may be relatively important for the force balance in

[1]This research was supported by National Key Basic Research Project: Research on the Formation Mechanism and Predication Theory of severe synoptic Disasters in China (CHERES, No. G1998040907) and by the National Natural Science Foundation of China under Grant Nos. 40075010 and 40028504.

[2]zmtan@netra.nju.edu.cn

the PBL. Recently a lot of approximate accelerating atmospheric boundary layer models have been developed for the different application. A relatively simple modified theoretical Ekman boundary-layer model including the inertial term with the geostrophic momentum approximation (GM) (Hoskins 1975) was proposed by Wu and Blumen (1982, hereafter WB). Assuming the condition of constant eddy viscosity, an analytical solution was obtained which extended the classical Ekman solution. Results of their study indicated that the wind structure in the PBL depends on the structure of geostrophic flow. However, the application of WB's modified Ekman boundary-layer model to the real case was bounded due to the constant turbulent exchange coefficient assumption (Levy 1989; Cullen 1989). Zhao (1988) extended the GM by including the Blackadar's general turbulent exchange coefficient (Blackadar 1979) to discuss the boundary-layer wind field in the PBL, whose numerical results further improved the wind structure in the analytical semi-geostrophic Ekman boundary-layer solution.

As shown in Ekman solution, the leading order flow in the PBL is the Ekman velocity, not the geostrophic flow; therefore, the GM is not just to the PBL motion. A so-called Ekman momentum approximation (hereafter EM) was suggested by Tan and Wu (1992, 1993), which extends the GM to the PBL. The EM matches the GM at the top of the boundary layer. Evidently the EM includes the more veracious accelerating flow than that in the GM model. However, so far only the simplified version of the EM has an analytical solution in which the turbulent friction terms were evaluated using the Ekman velocity (Tan and Wu 1992). Bannon (1998) gave a comparison of the EK, GM and EM with the theoretically primitive ageostrophic PBL model and showed that the EM model is a relative accurate approximate PBL model. However, his study is only limited in the two-dimensional and constant eddy viscosity case.

In the present study, an intermediate approximate PBL model based on the Ekman momentum approximation is developed, but the Blackadar's nonlinear eddy viscosity is incorporated to improve the Tan and Wu's (1993) theoretical model and Bannon's (1998) study. One might question why this kind of model is needed, since the three-dimensional numerical PBL model including the complex physical processes could simulate and predicate the three-dimensional wind structure in the PBL. In general, the three-dimensional numerical PBL model needs three-dimensional initial and boundary conditions and numerous calculations. The model developed in the present study needs only the two-dimensional geostrophic wind and its horizontal non-uniform distribution that can be provided by the large- and meso-scale model. Moreover, the boundary layer parameterizations are generally developed and tested primarily in one-dimensional model (Garratt 1994; Garratt et al. 1996), the present model obviously could provide an advanced base for this issue. On the other hand, so far the most PBL wind diagnostic models neglect the advection terms that could be improved by the present model, but its numerical complexity could be kept. Another reason for developing such simplified numerical model is associated with the recent atmospheric dynamics studies. For example, the most frontogenesis dynamic models, e.g., the semi-geostrophic theory (Hoskins and Bretherton 1972), do not incorporate the boundary layer process. Thus, it is necessary to develop a simple boundary layer model coupling with the semi-geostrophic frontogenesis model and to study the front-boundary layer dynamics (Blumen and Lundquist 2001).

Section 2 describes the equations of the intermediate PBL model with the Ekman momentum approximation and nonlinear eddy viscosity and boundary conditions. The numerical scheme for this model is given in section 3. Incomparsion of the EM with the EK and GM

in the barotropic and baroclinic conditions and the dynamic behaviors are presented in section 4. A summary is given in section 5.

2. Boundary layer model

Following Tan and Wu (1993), the PBL governing motion equation with the Ekman momentum approximation is given as

$$\left(\frac{\partial}{\partial t}+u\frac{\partial}{\partial x}+v\frac{\partial}{\partial y}\right)u_e-fv=-fv_g+\frac{\partial}{\partial z}\left(K\frac{\partial u}{\partial z}\right), \tag{1}$$

$$\left(\frac{\partial}{\partial t}+u\frac{\partial}{\partial x}+v\frac{\partial}{\partial y}\right)v_e+fu=fu_g+\frac{\partial}{\partial z}\left(K\frac{\partial v}{\partial z}\right), \tag{2}$$

$$\frac{\partial u}{\partial x}+\frac{\partial v}{\partial y}+\frac{\partial w}{\partial z}=0, \tag{3}$$

where (u, v) is the wind component in the (x, y) direction, f is the constant Coriolis parameter, (u_g, v_g) is the geostrophic wind, K is the vertical turbulent exchange coefficient for momentum, (u_e, v_e) denotes the x– and y–component wind speed in the classical Ekman model.

In order to solve Eqs.(1)–(2), the wind fileds at the lower and upper boundaries are required. The lower boundary condition is given by

$$z=0,\quad u=v=0, \tag{4}$$

and the upper boundary condition is

$$z=H_b,\quad u=u_T,\quad v=v_T, \tag{5}$$

where H_b is the depth of the boundary layer, here 2000 m is chosen, (u_T, v_T) is the wind speed at the top of the boundary layer that could be provided by the GM, and is different from that in the traditional Ekman–type PBL model. In the Ekman–type model, (u_T, v_T) is assumed to geostrophic wind (u_g, v_g).

The semi–geostrophic flow (u_T, v_T) at the top of the boundary layer can be determined by (1) and (2) when the turbulent friction is neglected, and then we have

$$\left(\frac{\partial}{\partial t}+u_T\frac{\partial}{\partial x}+v_T\frac{\partial}{\partial y}\right)u_g-fv_T=-fv_g, \tag{6}$$

$$\left(\frac{\partial}{\partial t}+u_T\frac{\partial}{\partial x}+v_T\frac{\partial}{\partial y}\right)v_g+fu_T=fu_g. \tag{7}$$

Solving (6) and (7), we have (u_T, v_T) as follow:

$$u_T=\frac{u_g-\frac{1}{f}\frac{\partial K_g}{\partial y}+\frac{1}{f^2}(v_g, u_g)_{ty}}{\Omega};\quad v_T=\frac{v_g+\frac{1}{f}\frac{\partial K_g}{\partial x}+\frac{1}{f^2}(u_g, v_g)_{tx}}{\Omega}, \tag{8}$$

where $\Omega=1+\frac{1}{f}\left(\frac{\partial v_g}{\partial x}-\frac{\partial u_g}{\partial y}\right)+\frac{1}{f^2}\left(\frac{\partial u_g}{\partial x}\frac{\partial v_g}{\partial y}-\frac{\partial u_g}{\partial y}\frac{\partial v_g}{\partial x}\right)$, $K_g=\frac{1}{2}(u_g^2+v_g^2)$, and $(A, B)_{ts}=\frac{\partial A}{\partial t}\frac{\partial B}{\partial s}-\frac{\partial B}{\partial t}\frac{\partial A}{\partial s}$.

The equivalent form of (1)–(2) may be rewritten as follow:

$$\begin{cases} \dfrac{\partial}{\partial z}\left(K\dfrac{\partial u}{\partial z}\right)+a_1u+b_1v=c_1\ , \\ \dfrac{\partial}{\partial z}\left(K\dfrac{\partial v}{\partial z}\right)+a_2u+b_2v=c_2\ , \end{cases} \tag{9}$$

where

$$\begin{cases} a_1=-\lambda\dfrac{\partial u_e}{\partial x}\ ,\ b_1=f-\lambda\dfrac{\partial u_e}{\partial y}\ ,\ c_1=fv_g+\lambda\dfrac{\partial u_e}{\partial t}\ , \\ a_2=-\left(f+\lambda\dfrac{\partial v_e}{\partial x}\right)\ ,\ b_2=-\lambda\dfrac{\partial v_e}{\partial y}\ ,\ c_2=-fu_g+\lambda\dfrac{\partial v_e}{\partial t}\ , \end{cases} \tag{10}$$

where λ is a control parameter. When $\lambda=0$, Eq.(9) reduces to the classical Ekman model in which the inertial terms are neglected, but for $\lambda=1$, (9) presents the modified Ekman boundary layer model with the Ekman momentum approximation. Moreover, Eq.(9) could be reduced to the semi-geostrophic Ekman boundary layer model (Eqs.(21a, b) in WB) when the classical Ekman flow (u_e, v_e) in (10) is replaced by the geostrophic flow (u_g, v_g).

In Eq.(9), the eddy diffusivity K generally should be a function of the wind and mixing length. Applying the general eddy viscosity expression in neutral conditions with the mixing-length approach (Blackadar 1979), we have

$$K=l^2\left[\left(\frac{\partial u}{\partial z}\right)^2+\left(\frac{\partial v}{\partial z}\right)^2\right]^{1/2}\ , \tag{11}$$

where l is a characteristic length scale of the turbulence momentum called the mixing length. A classical expression for l is proposed by Blackadar (1962) and it is

$$l=\frac{0.4(z+z_0)}{1+0.4(z+z_0)/\lambda}\ ,\quad \lambda=0.063\frac{u_*}{f}\ , \tag{12}$$

where λ is a maximum value reached at the top of the PBL, z_0 is the roughness length, $u_*=\left|\dfrac{\tau_0}{\rho}\right|^{1/2}=\left(K\left|\dfrac{\partial v}{\partial z}\right|\right)^{1/2}_{z=z_s}$ is the friction velocity, z_s is a height near the surface layer, $f=10^{-4}\ \mathrm{s}^{-1}$ taken at middle latitudes.

3. Numerical scheme

Equation (9), subject to the boundary conditions (4) and (5) and with eddy diffusivity (11), can be solved numerically when the geostrophic wind or the horizontal pressure gradients at the top of the boundary layer are given. Evidently (9) is one-dimensional for the boundary-layer wind at each horizontal grid point, which has few requirement of computational resources than that of the three-dimensional primitive PBL model, but includes the effects of horizontal inhomogeneity background wind by using the EM.

The numerical scheme for solving (9) adopted here is similar to that used by Zhao (1983). u and v are defined at the vertical grid point and eddy viscosity K at the half way between the vertical grid points. The turbulent stresses are defined at the same grid points as K. The successive approximation method has been used here. In order to solve (9), we solve firstly (9) with λ i.e. the classical Ekman solution, then substitute the classical Ekman solution into (10) and solve (9) with $\lambda=1$ again, and then obtain the Ekman momentum approximation solution.

4. Results and discussion

4.1 *Nonlinear steady barotropic case*

The barotropic boundary-layer wind structure and vertical motion at the top of the boundary layer with the constant and nonlinear eddy diffusivity for an ideal case are presented in this subsection. The barotropic geostrophic shear flow is given as

$$u_{g0} = u_0 - \alpha y; \quad v_{g0} = 0 \ , \tag{13}$$

where, α is a constant. $\alpha > 0$ represents the cyclonic shear flow, and $\alpha < 0$ denotes the anti-cyclonic shear flow. Consequently, the geostrophic vorticity is $\zeta_g = \alpha$. So (13) represents a constant vorticity shear flow. Here we set $u_0 = 20\ \mathrm{m\,s^{-1}}$, $\alpha = \pm\ 0.4f$ for the cyclonic and anticyclonic shear flow, respectively, and $f = 10^{-4}\ \mathrm{s^{-1}}$. Moreover, we select the point (0,0) to calculate the boundary-layer wind profile and the Ekman pumping velocity.

In order to validdte the numerical scheme for solving (9), the analytical solutions of the Ekman model (Eq.(4.5.31a) in Pedlosky 1987) and the semi-geostrophic Ekman boundary layer (see Eqs. (21a and b) in Wu and Blumen 1982) are applied to compare with the numerical solution of (9) for the constant-K case. Results illustrate the boundary-layer wind structure of analytical EK and GM solutions and numerical solution of (9) in the anticyclonic and cyclonic shear flow cases are quite similar, therefore the numerical scheme adopted here is reasonable.

Figures 1a and 1b show the wind hodograph in the EK, GM and EM models with the constant eddy viscosity for the cyclonic and anticyclonic shear cases, respectively. For the cyclonic shear flow, the boundary-layer wind speed in the EM is smaller than that in the EK, but larger than that in the GM (Fig. 1a). However, the EM's solution is larger than that in the EK and smaller than that in the GM for anticyclonic shear flow (Fig. 1b). The maximum improvement of the EM to GM occurs in the middle level of the boundary layer that is related to the effect of inertial acceleration. At the low-level the boundary-layer wind speed is relatively small that leads to a relative small inertial acceleration in both GM and EM, therefore the difference of wind speed between both models is relatively small. Otherwise, at the upper-level of the boundary layer the classical Ekman velocity (u_e, v_e) approaches to the geostrophic wind (u_g, v_g), therefore the inertial acceleration with the EM also tends to that with the GM. Therefore, the maximum departure of the EM from the GM occurs at the mid-level of PBL. Evidently the GM solution overestimates the effect of acceleration on the boundary-layer wind structure. Also the EK's solution overestimates the wind speed in the cyclonic shear and underestimates in the anticyclonic shear flow due to the neglecting of inertial terms.

The wind hodograph in the EK, GM and EM with the nonlinear eddy viscosity (10) for the cyclonic and anticyclonic shear flow is shown in Figs. 2a and 2b. Comparison of Figs. 2a and 2b with Figs. 1a and 1b shows that the boundary-layer wind speed is increased at the low-level and the angle between the wind vector near the surface and isobars is decreased by the nonlinear eddy viscosity, however the difference of boundary-layer wind structure between in the EM and in the GM is similar to that in the constant-K case.

In order to indicate the improvement of the wind speed in the EM to that in the GM and EK, a relative error of boundary layer wind speed in the GM and EK to that in the EM is

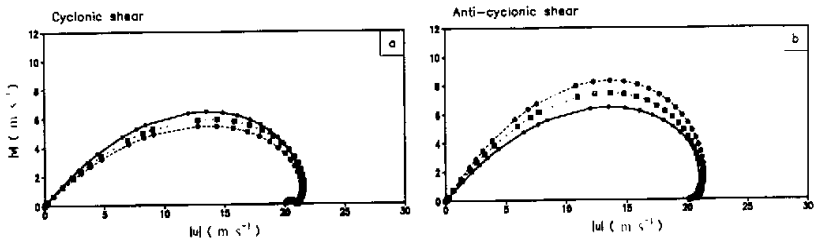

Fig. 1. The boundary-layer wind hodograph for numerical solution in the EK, GM and EM boundary layer model at point (0,0) for the cyclonic (a) and anticyclonic (b) shear flow. $K = 10$ $m^2 s^{-1}$. The solid, dashed and dotted lines represent the EK, GM and EM, respectively.

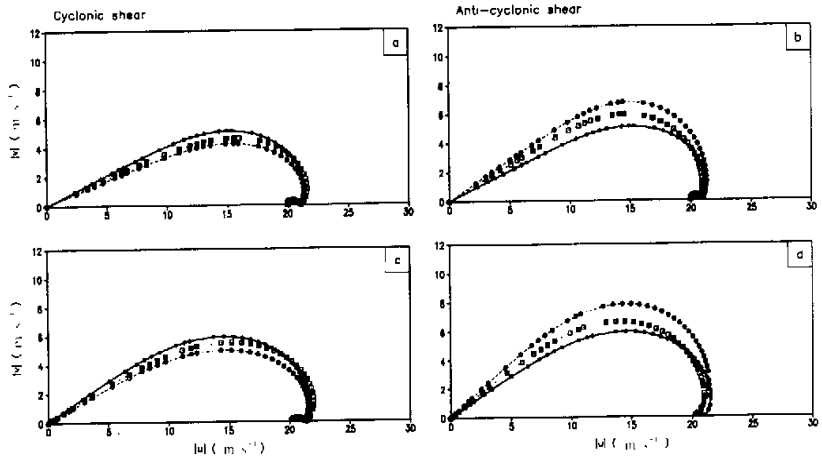

Fig. 2. Same as in Fig. 1, but for the nonlinear eddy viscosity. (a) Cyclonic shear, $z_0 = 1$ cm; (b) anticyclonic shear, $z_0 = 1$ cm; (c) cyclonic shear, $z_0 = 1$ m; (d) anticyclonic shear, $z_0 = 1$ m.

defined as follow:

$$RE_{GM\ EK} = \frac{\left|\vec{V}_{EM} - \vec{V}_{GM\ EK}\right|}{\left|\vec{V}_{EM}\right|}, \tag{14}$$

where $\vec{V}_{EM}$, $\vec{V}_{GM}$ and $\vec{V}_{EK}$ are the horizontal boundary-layer wind vectors in the EM, GM and EK, respectively.

Figures 3a and 3b show the RE_{GM} and RE_{EK} in the case of constant-K and nonlinear eddy viscosity, respectively. In Fig. 3 the solid and dashed lines represent the RE_{EK} and RE_{GM}, respectively. The thick and thin lines denote the cyclonic and anticyclonic shear flow, respectively. The relative errors are larger in the EK than that in the GM, and are also larger in the anticyclonic shear flow than that in the cyclonic one. Moreover the relative errors of the GM to the EM mainly occur at the surface and in the mid-level. Comparison of Fig. 3b with

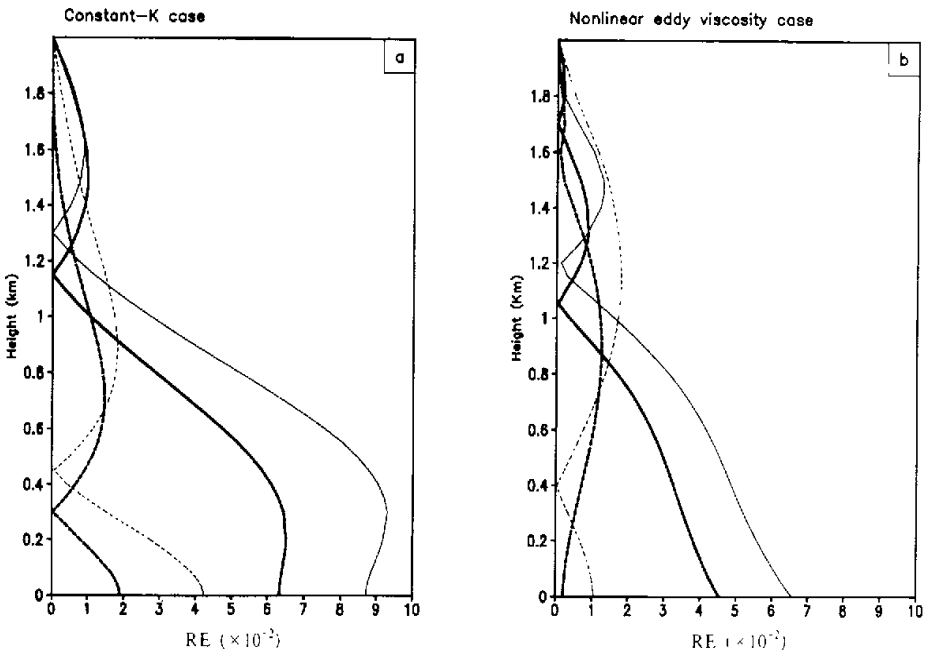

Fig. 3. The relative error (14) of the Ekman model and semi-geostrophic Ekman model to the Ekman momentum approximation boundary layer model. The solid and dashed lines represent RE_{EK} and RE_{GM}, respectively. The thick and thin lines denote the cyclonic and anti-cyclonic shear flow, respectively. (a) Constant-K, $K = 10\ m^2\ s^{-1}$; (b) nonlinear eddy viscosity for $z_0 = 1$ cm.

Fig. 3a illustrates that the nonlinear eddy viscosity could reduce the relative error RE_{EK} and RE_{GM}.

As shown in (10), the nonlinear eddy viscosity adopted here mainly depends on the vertical distribution of the wind and mixing length. The inertial acceleration affects not only the wind structure, but also the nonlinear eddy diffusivity. Figures 4a and 4b show the height-dependent profiles of nonlinear eddy diffusivity at point (0,0) in the cyclonic and anticyclonic shear flow for $z_0 = 1$ cm, respectively. The nonlinear eddy diffusivity in the EK, GM and EM models has a similar profile. The eddy diffusivity increases with height to a certain level at about 200 m, and then decreases from the maximum value to zero near the top of the model. The magnitude of nonlinear eddy viscosity is larger in the anticyclonic shear flow than that in the cyclonic one, which corresponds to the larger wind shear in the anticyclonic shear flow. Moreover, K in the EM is larger (smaller) than that in GM in the cyclonic (anticyclonic) shear flow. The maximum difference of K between in the EM and in the GM occurs at about the height of 800 m in the cyclonic shear and about 1000 m in the anticyclonic shear flow. Evidently, the turbulent exchange coefficient in the GM is hypocritically enhanced in anticyclonic shear flow and reduced in the cyclonic flow due to the overestimation of inertial affecting. We can also find that a lager surface roughness z_0 could lead to a larger turbulent exchange coefficient (Figs. 4c and 4d) and larger boundary-layer wind speed (Figs. 2c and 2d). The contribution of surface roughness z_0 to K in different models has a similar feature.

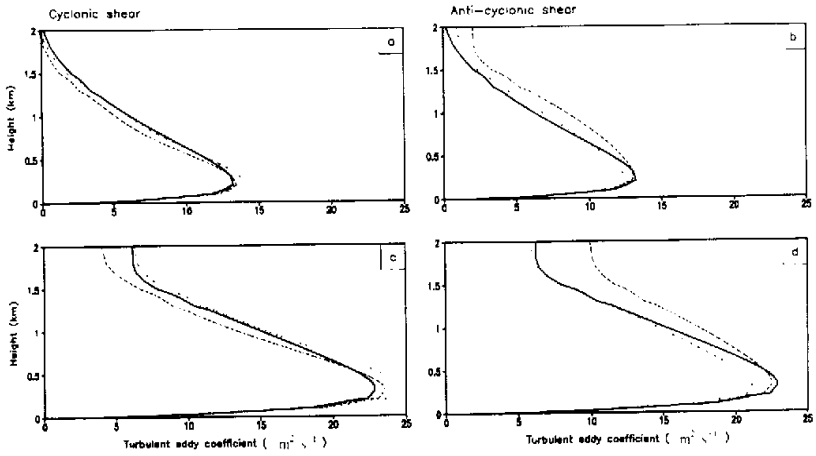

Fig. 4. The variation of nonlinear eddy viscosity with height at point (0,0). The parameters are the same as Fig. 2. The solid, dashed and dotted lines represent the solution of the EK, GM and EM, respectively. (a) Cyclonic shear, z_0 = 1 cm; (b) anticyclonic shear, z_0 = 1 cm; (c) cyclonic shear, z_0 = 1 m; (d) anticyclonic shear, z_0 = 1 m.

The vertical velocity at the top of the PBL, called Ekman pumping results from the convergence of Ekman flow because the boundary-layer friction is often applied as a lower boundary to the inviscid dynamics (Charney and Elissen 1949). In the classical Ekman model, the Ekman pumping is linearly dependent on the geostrophic vorticity at the top of the boundary layer (Holton 1992). Integrating the continue Eq.(3) with the assumption that the vertical motion is zero at the surface, we have the vertical motion in the boundary layer. The distributions of vertical motion at the top of the boundary layer at point (0,0) varying with the geostrophic vorticity in the EK, GM and EM are shown in Fig. 5. The solid, dashed and dotted lines represent the solution of the EK, GM and EM models, respectively. In general the vertical motion at the top of the boundary layer is increased with the cyclonic geostrophic vorticity increasing. In the EK, the pumping velocity is linearly dependent on the geostrophic vorticity, which is consistent with the analytical solution due to no acceleration flow affection. However, the pumping velocity in the EM is larger in the cyclonic (anticyclonic) shear case and smaller in the anticyclonic (cyclonic) one than that in the GM (EK), therefore the GM (EK) overestimates (underestimates) the effect of the acceleration flow on the pumping velocity. Figures 5b and 5c show the pumping in different PBL models for the nonlinear eddy viscosity. Comparison of Fig. 5b with Fig. 5a illustrates that the nonlinear eddy viscosity increases the vertical motion at the top of the boundary layer. Also the surface roughness z_0 could enhance the pumping velocity (see Fig. 5c).

4.2 *Nonlinear steady baroclinic case*

The role of baroclincity in the wind structure in the Ekman momentum approximation boundary layer model was discussed in this subsection. In general, the geostrophic wind is assumed to be a linear function of height z:

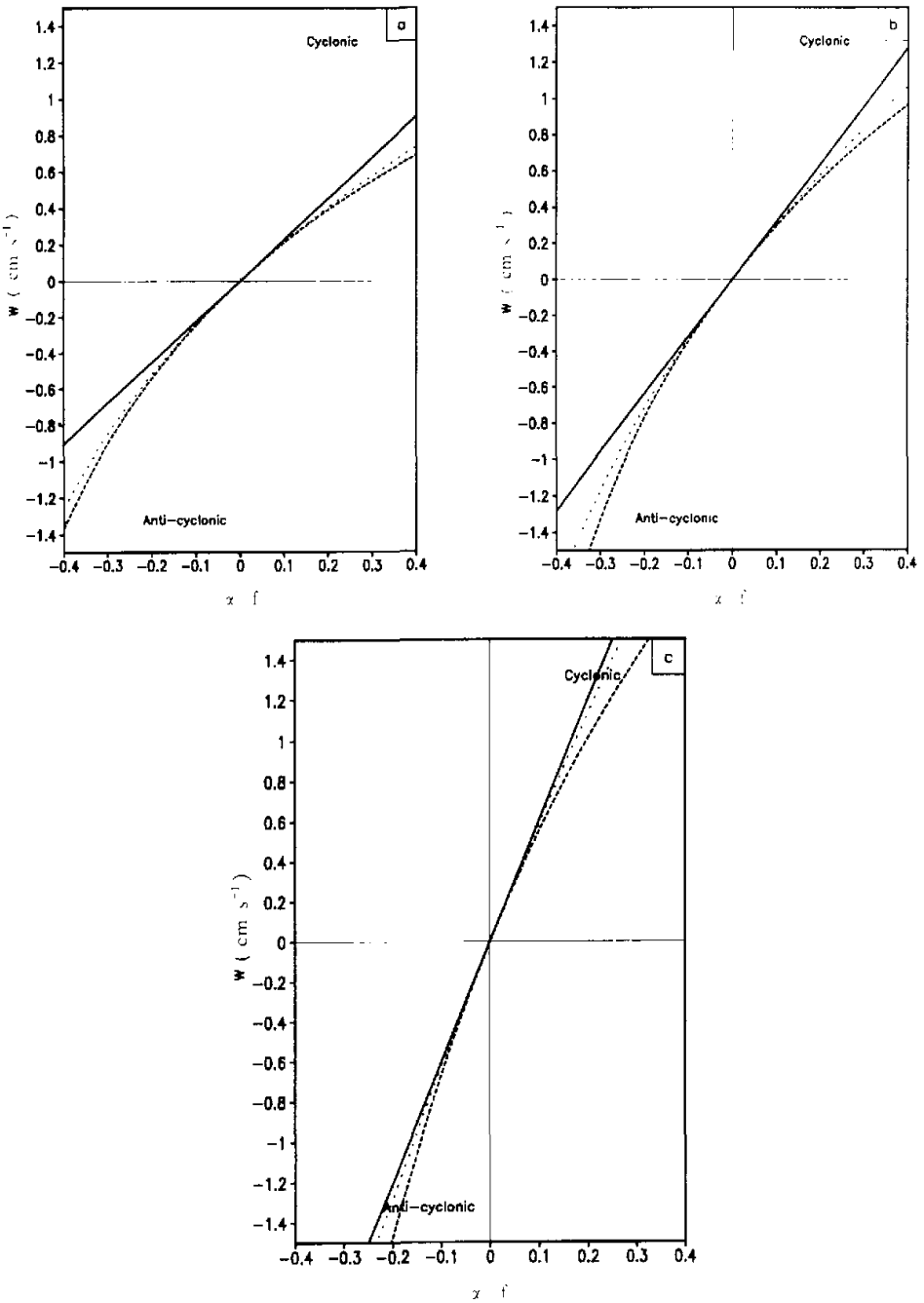

Fig 5. The vertical velocity at the top of the boundary layer varying with the geostrophic vorticity. The solid, dashed and dotted lines represent the solution of the EK, GM and EM models, respectively. (a) Constant eddy diffusivity; (b) nonlinear eddy diffusivity for z_0 = 1 cm, (c) nonlinear eddy diffusivity for z_0 = 1 m.

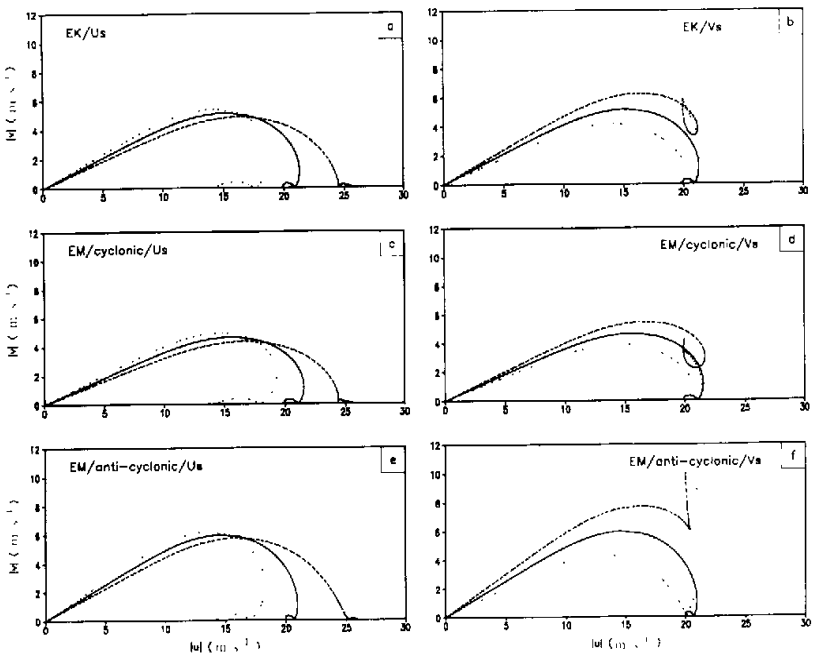

Fig. 6 The boundary-layer wind hodograph for baroclinic and nonlinear eddy viscosity EK and EM boundary layer models at point (0,0) in the cyclonic and anticyclonic shear flow $z_0 = 1$ cm. The solid line represents the barotropic boundary layer solution. The dashed and dotted lines represent the baroclinic boundary layer solution for the positive thermal wind shear ($u_s > 0$ or $v_s > 0$) and negative thermal wind shear ($u_s < 0$ or $v_s < 0$), respectively. Baroclinic Ekman model. (a) $u_s = \pm 2 \times 10^{-2}$ m s^{-2}, $v_s = 0$; (b) $u_s = 0$, $v_s = 2 \times 1^{-3}$ m s^{-2}; Baroclinic Ekman momentum approximation boundary layer model. (c) cyclonic shear, $u_s = \pm 2 \times 10^{-2}$ m s^{-2}, $v_s = 0$; (d) cyclonic shear, $u_s = 0$, $v_s = \pm 2 \times 10^{-2}$ m s^{-2}; (e) anticyclonic shear, $u_s = \pm 2 \times 10^{-2}$ m s^{-2}, $v_s = 0$. (f) anticyclonic shear, $u_s = 0$, $v_s = \pm 2 \times 10^{-2}$ m s^{-2}.

$$u_g = u_{g0} + u_s z \ , \quad v_g = v_{g0} + v_s z \ , \tag{15}$$

where $\vec{V}_s = (u_s, v_s)$ is the constant thermal wind shear that describes the baroclincity, $\vec{V}_{g0} = (u_{g0}, v_{g0})$ is the surface (barotropic) geostrophic wind as shown in (13).

Figure 6 shows the wind hodographs in the Ekman model and Ekman momentum approximation model for the baroclinic and nonlinear eddy viscosity case. The right and left panels of Fig. 6 denote the cases for $\vec{V}_{g0} \cdot \vec{V}_s \neq 0$ and $\vec{V}_{g0} \cdot \vec{V}_s = 0$, respectively. From Fig. 6 we can find that the effect of the acceleration in the EM on the boundary-layer wind structure in the baroclinic case is similar to that in the barotropic case. The acceleration flow in the EM results in the boundary-layer wind increasing in the anticyclonic shear flow and reducing in the cyclonic shear flow. Therefore, the Ekman momentum approximation model is also applied to the baroclinic boundary layer. The baroclinic boundary layer solution with the EM has both features of the classical baroclinic boundary layer solution and that associated with

the acceleration due to the Ekman momentum. Compared to the baroclinic EM solution, the GM solution also overestimates the effect of acceleration on the wind structure in the baroclinic PBL (figure not shown).

Comparison of Figs. 6c and 6d with Fig. 6a shows that the geostrophic wind decreasing with height ($u_s < 0$) and anticyclonic geostrophic shear are favorable to the formation of low-level jet (LLJ) in the PBL, however, the geostrophic wind increasing with height ($u_s > 0$) could reduce the LLJ. Comparison of Fig. 6f with Figs. 6b and 6d show that the anticyclonic shear could enhance the horizontal boundary-layer wind in the case of $v_s > 0$. These features are similar to the theoretical results in the baroclinic semi-geostrophic boundary layer model (Tan 2001).

The turbulent exchange coefficient in the EK and EM models for the baroclinic boundary layer is shown in Fig. 7. Compared with the barotropic case, the eddy viscosity is enhanced when the geostrophic wind increases with height ($u_s > 0$), and decreases in the case of $u_s < 0$. The maximum differences of K between the barotropic and baroclinic boundary layer are about 15% appear at the height of 200–300 m where the maximum value of K appearing for the present case. However, the thermal wind shear v_s could not alter the maximum value of K and only changes the vertical distribution of eddy viscosity.

5. Summary and conclusion

A quasi three-dimensional intermediate numerical PBL model is developed by including the inertial acceleration under the Ekman momentum approximation and the Blackadar's

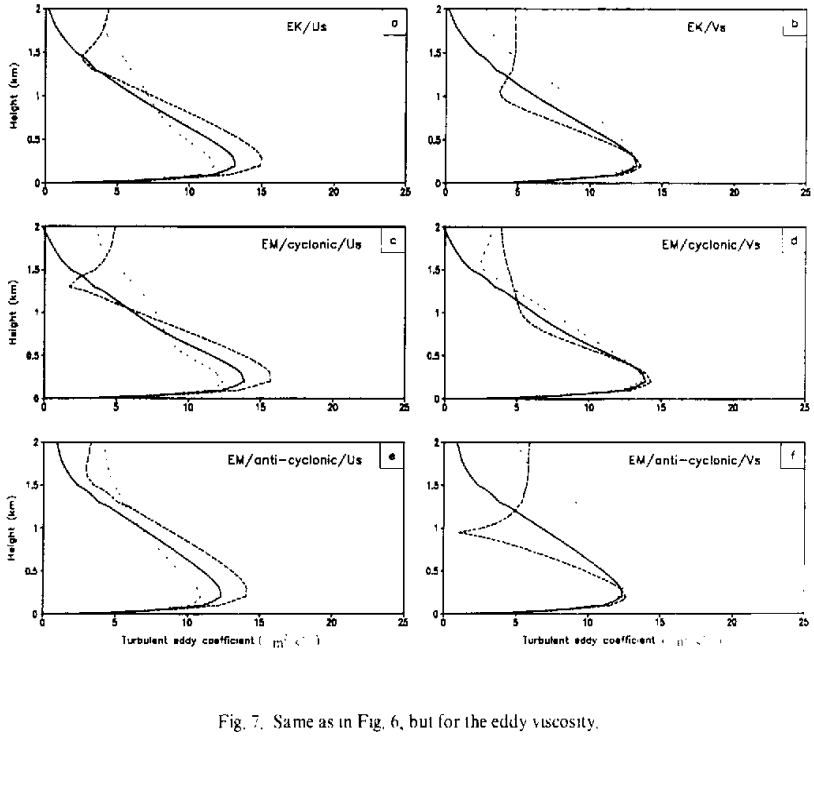

Fig. 7. Same as in Fig. 6, but for the eddy viscosity.

nonlinear eddy viscosity, which further improved the theoretical model proposed by Tan and Wu (1993). Compared with the quasi three-dimensional numerical PBL model and the traditional PBL wind diagnostic model, the EM has more advantages in the numerical calculation and the included dynamic processes. For example, the EM is one-dimensional at each horizontal grid point for the predication of wind field in the PBL, and has less computerable cost than the three-dimensional primitive PBL model. To the traditional PBL wind diagnostic model, the EM includes the acceleration effect.

Compared with other simplified PBL models, e.g. the classical Ekman (EK) and geostrophic momentum approximation (GM) PBL models, the EM is accurate in the predication of wind fields in the PBL. The GM has an overestimated acceleration affection on the PBL flow that results in an underestimation (overestimation) of the wind speed and vertical motion at the top of the boundary layer in the cyclonic (anticyclonic) shear flow, however, the classical Ekman model overestimates (underestimates) the wind speed and pumping velocity in the cyclonic (anticyclonic) shear flow due to the neglecting of acceleration flow. These features are similar to that in Bannon (1998). The maximum difference in the wind speed and eddy viscosity between in the EM and in the GM occurring at the mid-level of the PBL results from different acceleration affections included. Of course, the differences could be reduced in the nonlinear turbulent exchange coefficient case. Moreover, the nonlinear eddy viscosity increases the pumping velocity at the top of the boundary layer in these simplified boundary layer models.

The Ekman momentum approximation boundary layer model could be also applied to the baroclinic atmospheric boundary layer. The thermal wind shear has no more effect on the acceleration flow, but more on the eddy viscosity in the present case. The decreasing of geostrophic wind and anti-cyclonic shear is favorable to the formation of low-level jet in the PBL.

Because the numerical complexity in the EM is similar to that in the classical Ekman model, the present model may be easily extended to the nonsteady case including the thermal process and other physical processes. Further studies should be carried out, such as, coupling the present model with the frontogenesis' model that is used to study the effects of the boundary-layer friction on the frontal circulation in the PBL.

The authors would like to acknowledge the assistance provided by Professor Zhao Ming.

REFERENCES

Bannon, P. R., 1998: A comparison of Ekman pumping in approximate modes of the accelerating planetary Boundary layer. *J. Atmos. Sci.*, **55**, 1446-1451.

Blackadar, A. K., 1962: The vertical distribution of wind and turbulent exchange in a neutral atmosphere. *J. Geophys. Res.*, **67**, 3095-3102.

Blackadar, A. K., 1979: High-resolution models of the planetary boundary layer. *Advances in Environmental Science and Engineering*, 1, No. 1, J. R. Pfafflin and E. N. Ziegler, Eds., Gordon and Briech Sci. Publ. New York, 50-85.

Blumen, W., and J. K. Lundquist, 2001: Spin-up and spin-down in rotating fluid exhibiting inertial oscillations and frontogenesis. *Dyn. Atmos. Oceans*, **33**, 219-237.

Charney, J. G., and A. Eliassen, 1949: A numerical method for predicting the perturbations of middle-latitude westerlies. *Tellus*, **1**, 38-54.

Cullen, M. J. P., 1989: On the incorporation of atmospheric boundary layer effects into a balanced model. *Quart. J. Roy. Meteor. Soc.*, **115**, 1109-1131.

Ekman, V. W., 1905: On the influence of the Earth's rotation on ocean-currents. *Arch. Math. Astron. Phys.*, **2**(11), 1-53.

Garratt, J. R., 1994: *The Atmospheric Boundary Layer*. Cambridge University Press, Cambridge, U. K. 316pp.

Garratt, J. R., G. D. Hess, W. L. Physick, and P. Bougeault, 1996: The atmospheric boundary layer – Advances in knowledge and application. *Bound.-Layer Meteor.*, **78**, 9–37.

Holton, J. R., 1992: *An Introduction to Dynamic Meteorology*, 3rd ed. Academic Press, 570pp.

Hoskins, B. J., 1975: The geostrophic momentum approximation and the semi-geostrophic equations. *J. Atmos. Sci.*, **32**, 233–242.

Hoskins, B. J., and F. P. Bretherton, 1972: Atmospheric frontogenesis models: Mathematical formulation and solution. *J. Atmos. Sci.*, **29**, 11–37.

Levy, G., 1989: Surface dynamics of observed maritime fronts. *J. Atmos. Sci.*, **46**, 1219–1232.

Pedlosky, J., 1987: *Geophysical Fluid Dynamics*, 2nd ed. Springer-Verlag, 710pp.

Tan Zhemin, and Wu Rongsheng, 1992: Dynamics of Ekman momentum flow and frontogenesis. *Science in China*, **B35**, 117–128.

Tan Zhemin, and Wu Rongsheng, 1993: The Ekman momentum approximation and its application. *Bound.-Layer Meteor.*, **68**, 193–199.

Tan Zhemin, 2001: An Approximate analytical solution for baroclinic and variable eddy diffusivity semi-geostrophic Ekman boundary layer. *Bound.-Layer Meteor.*, **98**, 361–385.

Wu, R., and W. Blumen, 1982: An analysis of Ekman boundary layer dynamics incorporating the geostrophic momentum approximation. *J. Atmos. Sci.*, **39**, 1774–1782.

Zhao Ming, 1983: The theoretical distribution of wind in the planetary boundary layer with circular isobars. *Bound.-Layer Meteor.*, **26**, 209–226.

Zhao Ming, 1988: A numerical experiment of the PBL with geostrophic momentum approximation. *Advances in Atmospheric Sciences*, **5**, 47–56.

Ekman 动量近似下中间边界层模式中的风场结构

谈哲敏 王 元

P425 A

摘 要

发展了一个准三维的、中等复杂的边界层动力学模式，该模式包含了 EKman 动量近似下的惯性加速度和 Blackadar 的非线性湍流粘性系数，它进一步改进了 Tan 和 Wu(1993)提出的边界层理论模型。该模式在数值计算复杂性上与经典 Ekman 模式相类似，但由于包含了 Ekman 动量近似下的惯性项，使得该模式比传统 Ekman 模式更近于实际过程。文中详细地比较了该模式与其他简化边界层模式在动力学上的差异，结果表明：在经典的 Ekman 模式中，由于忽略了流动的惯性项作用，导致在气旋性切变气流(反气旋性切变气流)中风速和边界层顶部的垂直速度的高估(低估)，而在半地转边界层模式中，由于高估了流动惯性项的作用，结果与经典 Ekman 模式相反。同样，该模式可以应用于斜压边界层，对于 Ekman 动量下的斜压边界层风场同时具有经典斜压边界层和 Ekman 动量近似边界层的特征。

关键词：风场结构，Ekman 动量近似，边界层模式